Optogenetically-Induced Population Discharge Threshold as a Sensitive Measure of Network Excitability

Klorig, D.C.[1,2], Alberto, G.E.[1,2], Smith, T.[1], Godwin, D.W.[1-3]

[1]Department of Neurobiology and Anatomy, [2]Neuroscience Program, [3]Department of Physiology and Pharmacology
Wake Forest University, Winston-Salem, North Carolina, USA

Abstract

Network excitability is governed by synaptic efficacy, intrinsic excitability, and the circuitry in which these factors are expressed. The complex interplay between these factors determines how circuits function, and at the extreme, their susceptibility to seizure. We have developed a novel optogenetic intensity response procedure that provides a sensitive, quantitative estimate of network excitability. By combining optogenetic stimulation of the hippocampus with chronic multi-site recordings in peri-hippocampal structures of awake behaving mice, we induced abnormal network-wide epileptiform population discharges (PD) that were nearly indistinguishable from spontaneously occurring interictal spikes. By systematically varying light intensity, and therefore the magnitude of the optogenetically-mediated current, we generated intensity-response curves using the probability of PD as the dependent variable. This probability curve was well fit by a Boltzmann function, from which we calculated the intensity that produces a half-maximal probability of discharge (I50). This novel metric, the I50, is correlated with the optogenetic after-discharge threshold (oADT) in the same mice. Manipulations known to increase excitability, such as sub-convulsive doses (20 mg/kg) of the chemoconvulsant pentylenetetrazol (PTZ), produced a leftward shift in the curve compared to baseline. The anti-epileptic drug levetiracetam (40 mk/kg), in combination with PTZ, produced a rightward shift. Optogenetically-induced population discharge threshold (oPDT) baselines were stable over time, suggesting the metric is appropriate for within-subject experimental designs with multiple pharmacological manipulations. The oPDT is a sensitive measure of subconvulsive network excitability, with broad applicability to a number of areas of investigation.

Significance Statement

Network excitability is carefully regulated by homeostatic mechanisms in the brain in order to maintain optimal functional conditions. Abnormal excitability is associated with a number of neurological disorders including epilepsy. Excitability can be measured in single cells *in vitro*, but it is difficult to extrapolate from these values to the functional impact on the network as a whole. Epileptiform discharges are network wide events that represent a distinct transition from normal to abnormal functional modes. We developed a new technique that uses light intensity-response curves to precisely determine the threshold for this transition as a surrogate measure of network excitability and seizure susceptibility.

Introduction

Models of epileptogenesis, involving spontaneous seizure, are preferred for testing the effectiveness of therapeutic interventions because of their presumed similarity to the disease in humans (Lévesque and Avoli, 2013). However, the unpredictable nature of spontaneous seizure makes it difficult to study, at a mechanistic level, why a particular intervention is effective. Furthermore, because of variability in seizure expression, these models are time consuming to implement, require constant video-EEG monitoring, prolonged drug administration, and large numbers of animals (Löscher, 2011). Models of acute seizure offer a more controlled platform for measuring seizure susceptibility and the effectiveness of intervention but suffer from a strong dependence on the nature of the seizure induction method. Previously, the transition between normal and epileptiform activity has been estimated by measuring behavioral seizure thresholds or after-discharge thresholds (ADT), by chemical modification of the balance of excitation and inhibition, or by repetitive electrical stimulation of the brain with increasing amounts of current (Spiegel, 1937; Ziskind et al., 1946; Swinyard et al., 1952; Barton et al., 2001). Chemical and electrical methods for measuring seizure susceptibility lack spatial and cellular specificity and are therefore imprecise with regard to the specific neural pathways and cellular contributions being investigated (Histed et al., 2009). The ambiguity in site of action, and the uncertain relationship between dose or current and the resulting seizure makes it difficult to interpret such experiments mechanistically.

We developed a new approach for quantifying network excitability, in vivo, using an optogenetic light intensity-response curves that allows for independent measurement of excitability and seizure susceptibility. Optogenetic methods are well-suited to exploring the effects of abnormally synchronous firing on brain networks because they allow for simultaneous modulation of a defined population of cells (Khoshkhoo et al., 2017; Osawa et al., 2013; Weitz et al., 2015). We present two complimentary methods for determining optogenetic thresholds in chronically implanted mice, one for interictal spikes (IIS) and one for acute seizures. The first, the optogenetic population discharge threshold (oPDT), is a novel approach to measuring IIS thresholds using a single light pulse of varying intensity and accounts for the probabilistic expression of the IIS. We use the term population discharge (PD) instead of IIS to indicate that the discharges are experimentally generated and not necessarily associated with seizure. By using established pharmacologic modulators of excitability we demonstrate that the oPDT is dependent on circuit level excitability.

Because PDs are discrete events, the oPDT can be monitored over long time scales with high temporal resolution to fully capture the dynamics of network excitability, a property difficult to measure in awake behaving animals. The second is the optogenetic after-discharge (AD) threshold (oADT), and is based on established electrical ADT protocols, but by varying light intensity rather than electrical current. We show that train stimuli with light of a sufficient intensity produces a robust oAD and kindling with daily oADs results in overt behavioral seizure.

We show that the oADT and the oPDT, in the same animals, are equivalent in terms of light intensity. The oADT, however, requires an additional accumulating process involving multiple oPDs in a short period of time. Comparing the two metrics allows for separation of the contribution of excitability and seizure susceptibility, features that are inseparably intertwined in other measures of seizure threshold. Finally, because the oPDT does not involve the generation of an AD, it may also be a useful measure of excitability in a range of normal and pathologic conditions other than seizure.

Materials and Methods

Subjects. Male Thy1-ChR2-YFP (founder line 18) transgenic mice (Arenkiel et al., 2007; Wang et al., 2007) (Stock # 007612, The Jackson Laboratory) were used for chronic optogenetic stimulation and recording (n = 35). Thy1 line 18 mice express wildtype ChR2 fused to EYFP in area CA1, subiculum, and layer 5 of cortex (Arenkiel et al., 2007). In area CA1, expression is specific to excitatory pyramidal neurons and is concentrated in calbindin-negative cells in the deep pyramidal cell sublayer (**Fig. 1c**) (Dobbins et al., 2018). These mice can be bred as homozygotes, ensuring consistent expression levels and patterns from animal to animal, a significant advantage for reproducibility. For this reason, they are used in a number of optogenetics studies (Ting and Feng, 2013). Not all animals were used for all experiments; exact numbers are reported throughout. All animal experiments were approved by the Institutional Animal Care and Use Committee (IACUC) of Wake Forest University and in agreement with National Institutes of Health and United States Department of Agriculture guidelines, including practices to eliminate suffering and minimize animal numbers.

Chronic Implant. Details of the implantation surgery and chronic recording array are described in a previous publication (Klorig and Godwin, 2014). Briefly, Thy1 mice (age 2-9 months, mean 120 ± 9 days) were anesthetized with isoflurane and placed in a stereotaxic device. All surgical procedures were performed under red light to avoid sustained activation

of ChR2. Metal ground screws were secured to the cranium bilaterally so that they were in contact with the subarachnoid space posterior to the transverse sinus. A total of 8 tungsten microwires were implanted in a satellite array in cortical, subcortical, and hippocampal locations: prefrontal cortex, (PFC, AP: 5.58, L: 0.37, DV: -1.81, in mm, from the interaural plane), anterior medial thalamic nucleus (AM, AP: 2.86, L: 0.24, DV: -3.62), dentate gyrus (DG, AP: 1.50, L: 1.39, DV: -1.61), hippocampus (CA3, AP: 1.34, L: 2.88, DV: -2.12), entorhinal cortex (Ent, AP: 0.19, L: 3.90, DV: -2.73, angled 16° posterior), subiculum (sub, AP: 0.88, L: 1.02, DV: -1.43), and left CA1(AP: 1.00, L: -2.36, DV: -1.20). (Fig. 1A). A magnetic rotary fiber connector with an attached microwire (optrode) was placed in intermediate CA1 near subiculum (CA1a) (AP: 1.00, L: 2.36, DV: -1.20, from the interaural plane). The stimulation fiber was a multimodal fiber with a 200 µm diameter core and a numerical aperture of 0.39 (FT200UMT, ThorLabs). The recording electrode extended 0.5 mm beyond the fiber tip. The fiber optic was situated 0.4 mm dorsal to the pyramidal cell layer and 0.3 mm dorsal to the basal dendrites. The optrode was configured to minimize the photovoltaic effect (<0.02% LFP amplitude) by cutting the electrode at an angle so that the exposed metal surface was not directly illuminated by the implanted fiber (Cardin et al., 2010). Wild-type (n = 2) and post-mortem control (n = 4) recordings were used to confirm the absence of artifact. This setup allowed for high quality recordings, free of movement artifacts, even during behavioral seizure.

Light stimulation and recordings. Mice were allowed to recover 1 week prior to recordings. Wideband (0.3-20kHz, sampled at 40kHz) depth recordings were made using the SciWorks recording system (DataWave Technologies), AM-3600 extracellular amplifiers (A-M Systems), and T8G100 headstage amplifiers (TBSI). Photostimulation was performed with a fiber-coupled LED with peak emission at 470 nm (M470F3, ThorLabs). LED intensity was controlled using an LED driver with analog modulation (LEDD1B, ThorLabs). Analog output pulses were generated within SciWorks and used to control the LED driver. Light pulses were continually monitored with a silicon photodiode placed near the emitter. A custom op-amp based current-to-voltage converter circuit was used to linearize the photodiode output and the resulting signals were recorded along with the electrophysiology data. Two measures of light output are provided; the power (mW) at the tip of the source fiber and an arbitrary linearized scale (see **Fig. 3a** for further explanation). Light power ranged from 0.43 – 4.15 mW at the fiber tip corresponding to an irradiance of 0.2 – 1.96 mW/mm^2 at the recording site estimated using the empirically derived model described in (Aravanis et al., 2007; Yizhar et al., 2011).

Video and Behavioral Scoring. Recording sessions were video recorded and an infrared LED synchronized to the stimulus onset was placed in view of the video camera for precise temporal alignment between the video and the

recordings. Video was used for assessment of behavioral seizure using a modified Racine scale (Pinel and Rovner, 1978; Racine, 1972a). Latencies to seizure stage relative to the onset of the stimulus and durations were also recorded.

Histological Verification of Electrode Placement. On completion of recording experiments, mice were anesthetized with Euthasol (Virbac Animal Health), electrolytic lesions were performed at each electrode site (20 nA, 10 sec), then animals were transcardially perfused with saline and 4% paraformaldehyde solution in PB. After removal and post-fixing, brains were sectioned in 50 µm slices using a vibratome. The slices were then mounted on slides and stained using cresyl violet (Nissl). Each slice was imaged using a light microscope and the stereotaxic coordinates of each electrode were recorded. Animals were excluded from further analysis if electrodes utilized in those analyses were located outside of the target areas (n = 5).

Confocal Microscopy. ChR2-eYFP expression in Thy1 mice was imaged in non-implanted animals. Confocal imaging was performed on a Zeiss LSM 710 confocal microscope with 10X, 20X air and 60X water immersion objectives.

Experimental Design and Statistical Analysis. Data analysis was performed using custom scripts written in MATLAB (MathWorks). The suite of stimulus presentation and analysis tools used to generate and calculate the oPDT is available on github (https://github.com/neuroptics/optoDR).

Optogenetic After-Discharge Threshold (oADT) and Kindling Procedure. oADTs were determined by presenting optical stimulation trains at 6.67 Hz (10 s duration, 4 ms pulse, 150 ms interval, 66 pulses), then increasing the intensity (with a 2 min interval) until an AD was evoked (characterized by high amplitude, self-sustaining activity that persisted > 5 s after the stimulus ended). A modified optogenetic kindling procedure was used that allowed for estimation of oAD thresholds, involving repeated daily light stimulation at increasing intensity until an AD was evoked (with intensities identical to that performed on the first day), similar to established procedures (Bragin et al., 2002; Pinel et al., 1976). ADs were defined as sustained high-amplitude spike and poly-spike activity lasting at least 5 sec following termination of the stimulus. oAD durations were measured from the start of the stimulus to the last spike of the oAD. Only one oAD was evoked per 24 hour period. This procedure was repeated each day for 15 days.

Optogenetic Population Discharge (oPD) Intensity-Response Curve. Square pulses (10 ms) of light were delivered at a range of intensities (20 levels, 0.43 - 4.15 mW at fiber tip, 0.2 – 1.96 mW/mm^2 at the recording site). Sixty repetitions of each intensity were presented in randomly ordered blocks with a 1 s or 3 s interval between pulses. A timing pulse was used to precisely align responses to the onset of the LED. For the epileptiform discharge curves, time-locked evoked

responses were extracted, the 2nd derivative calculated, and a sliding window (10 ms) was used to calculate instantaneous root-mean-square (RMS) power via convolution. The max RMS within a specified time window was calculated, sorted by magnitude, and plotted for each channel over all stimulation levels. The channel with the sharpest transition between sub-PD and PD was chosen and the threshold set (typically contralateral CA1, but occasionally DG or CA3 were chosen). All subsequent analyses for a given animal were performed with the same channel and threshold. PD detection was verified visually (see **Fig. 2b-d**). The ratio of PD events per level (out of 60 repetitions) was calculated to generate a probability curve. This curve was fit by the Hodgkin and Huxley formulation of the Boltzmann distribution:

$$f(x) = \frac{1}{1 + e^{\left(\frac{a-x}{b}\right)}}$$

where a is the I50, and b is the slope (Hodgkin and Huxley, 1952)(**Fig. 3h**), using nonlinear regression (least squares) in MATLAB. The I50 value for each session was then used for further comparisons.

Pharmacology. All experiments utilized a within-subjects design. Treatments were compared to a pre-treatment baseline using repeated measures one-way ANOVA with Tukey's test for multiple comparisons. Saline controls were also performed and compared to pre-injection baselines.

Statistics and Measures of Reliability. Statistical testing was performed with MATLAB and Prism (GraphPad). All means are reported ± SD, with 95% confidence intervals (CI) where appropriate. Data sets were tested for normality using the omnibus K^2 test (D'Agostino et al., 1990). Comparisons were performed using repeated measures one-way ANOVA with Tukey's test for multiple comparisons, paired t-tests, Fischer's exact test, or Wilcoxon matched pairs test where appropriate. Correlation coefficients were calculated using Pearson's or Spearman's method where appropriate. All reported statistics are labeled with the test used. Box and whisker plots have min-max whiskers, 25th to 75th percentile boxes, and the central line is the median. The probability of oAD given at least x oPDs was calculated using the formula: $P(AD|\sum PD_i \geq x) = \frac{P(AD \cap \sum PD_i \geq x)}{P(\sum PD_i \geq x)}$. For assessment of oAD probability given oPD on a given stimulus pulse n, we used the formula for conditional probability: $P(AD|PD_n) = \frac{P(AD \cap PD_n)}{P(PD_n)}$. For assessment of oPD_{I50} probabilities given the results of previous trials we used the formula: $P(PD_{\mathrm{I50}}|PD_{n-\mathrm{back}}) = \frac{P(PD_{I50} \cap PD_{n-\mathrm{back}})}{P(PD_{n-\mathrm{back}})}$. Fisher's exact test was used to compare proportions.

Results

In order to explore network propagation of optogenetically induced seizure and PD activity, we developed a multi-site satellite array system consisting of individually placed microwires in perihippocampal structures and an optrode above CA1. Targets included prefrontal cortex (PFC), anterio-medial thalamus (AMTh), entorhinal cortex (Ent), dentate gyrus (DG), subiculum (Sub), hippocampal area CA3 (CA3), and area CA1 bilaterally (CA1-L and CA1-R) (**Fig. 1a)**). These recording sites provide coverage of areas demonstrated to be strongly activated by optogenetic stimulation of CA1 using fMRI (Weitz et al., 2015). Our preparation yielded high quality chronic recordings of multiple interconnected areas, allowing us to assess the impact of optogenetic stimulation on the network.

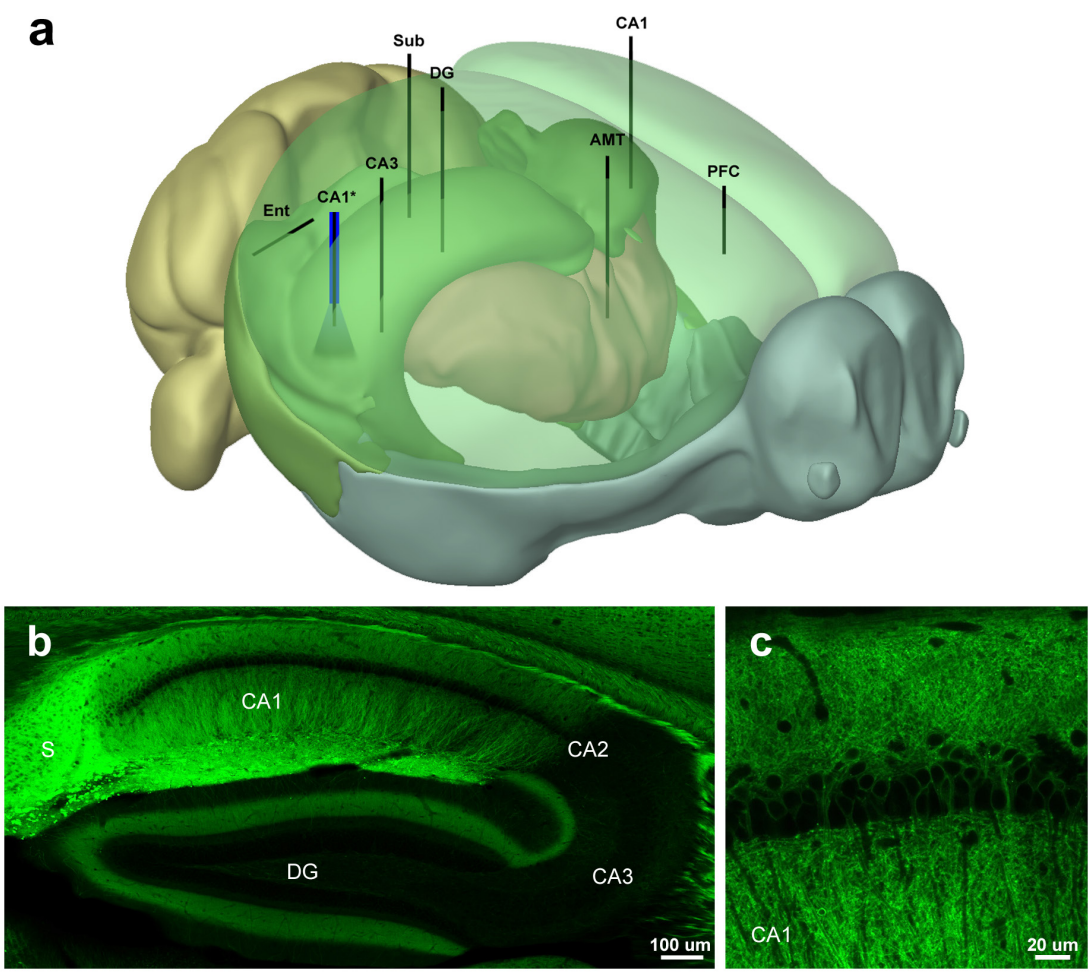

Figure 1 | Electrode placement and expression patterns in the Thy1-ChR2 (line 18) mouse. (**a**) Schematic showing the placement of the electrode array and optrode. (**b**) Distribution of ChR2-EYFP in the hippocampus of the Thy1 (line 18) mouse. Note high expression levels in CA1 and subiculum. 10x tiled confocal image. (**c**) ChR2-EYFP is expressed in deep pyramidal neurons in CA1 (Dobbins et al., 2018). 63x oil immersion confocal image. The 3D model was generated using Brain Explorer Software courtesy of the Allen Brain Institute (http://mouse.brain-map.org/static/brainexplorer).

Measuring the oADT and opto-Kindling

Using this preparation, we measured optogenetic after-discharge thresholds (oADT) by varying the intensity of light stimulation. We used rhythmic squarewave optical stimuli (6.67 Hz, 10 ms pulse, 10 sec train) to induce optogenetic AD

and behavioral seizure. 6.67 Hz was the lowest frequency that reliably produced an oAD and the longer period (150ms) provides sufficient time between pulses to observe the propagation of induced activity throughout the network (**Fig. 2b**). We measured oAD thresholds by presenting stimulus trains every 2 minutes at increasing light intensity until an oAD occurred (**Fig. 2a-c**). Subthreshold stimulation produced local activation at the stimulation site (CA1), but the activity did not spread to downstream areas (**Fig. 2a**, top inset). The mean oAD threshold was 2.11 mW (SD 1.12, 95% CI [1.08- 3.15], *n*=7).

Our preparation is configured to stimulate CA1 without damaging it by situating the fiber optic just above CA1 in visual cortex. In addition to strong expression in CA1, Thy1 mice also express ChR2 in layer 5 of cortex, raising the possibility that these cells were activated by light backscatter. To verify that CA1 is the relevant site of stimulation for seizure induction, we performed control experiments (n = 2) in which the fiber was placed superficially in cortex (0.5mm dorsal to the fiber location in the standard array). Much higher light intensities were required to induce seizure in these animals (16.58 mW and 27.86 mW using a fiber coupled laser), levels sufficient to produce suprathreshold activation of CA1 from this distance, suggesting that activation of cortex is not sufficient to produce seizure and that CA1 is the primary site of activation.

Occasionally the stimulation intensity just below threshold produced synchronous discharges similar to oPDs (see **Fig. 3** for detection parameters) on the first few pulses but not subsequent pulses (**Fig. 2a**, red traces, top inset, also see **Fig. 5**). Suprathreshold stimulation produced network wide oPDs following each pulse, high-frequency high-amplitude bursts, and oAD. The probability of oAD increased with the number of oPDs generated by the stimulus (**Fig. 2c**), P(AD) > 0.90 for *x* = 8 oPDs and P(AD)>0.99 for *x* = 17 oPDs (n = 841 stimulus trains). For subthreshold stimuli, the probability of an oPD drops off with pulse number, likely due to desensitization of ChR2 (**Fig. 2c** inset). oADs occurred during and immediately after stimulation (**Fig. 2a-c**), rather than after a delay as previously observed with optogenetic seizure induction in motor cortex (Khoshkhoo et al., 2017). The mean oAD duration was 23.1 sec (SD 4.84, 95% CIs [22.2, 24.0], *n* = 105 oADs).

High frequency oscillations (80-500 Hz) have been detected preceding seizures in a number of animal models and in intracranial recordings from humans with epilepsy (Bragin et al., 1999; Staba et al., 2002; Zijlmans et al., 2012). In the majority (88%, *n* = 105 oADs) of optogenetically induced oADs, high-frequency, high amplitude oscillations occurred

in CA3, DG, and CA1 (**Fig. 2a and b**). A non-zero phase shift was observed between these areas suggesting synaptic or ephaptic transmission, rather than volume conduction (Shivacharan et al., 2019) (**Fig. 2b**). The mean latency from the start of the stimulation to burst onset was 6.42 s (SD 2.75, 95% CI [5.87-6.97], *n* = 97 oADs). Epileptiform bursts ranged in frequency from 150 to 400 Hz (6.6 to 2.5-ms intraburst intervals) and were detected in all animals tested (7/7). These bursts were similar (in terms of amplitude and frequency) to patterns previously observed in perforant path stimulated or kainate treated rats (Bragin et al., 1997, 2004, 2005).

Network wide oPDs occurred on the first pulse of the stimulus train, however, the seizure itself required multiple oPDs to become self-sustaining (Fig. 2c). This suggests that repeated oPDs, rather than simply repeated stimulation, were required to generate an oAD.

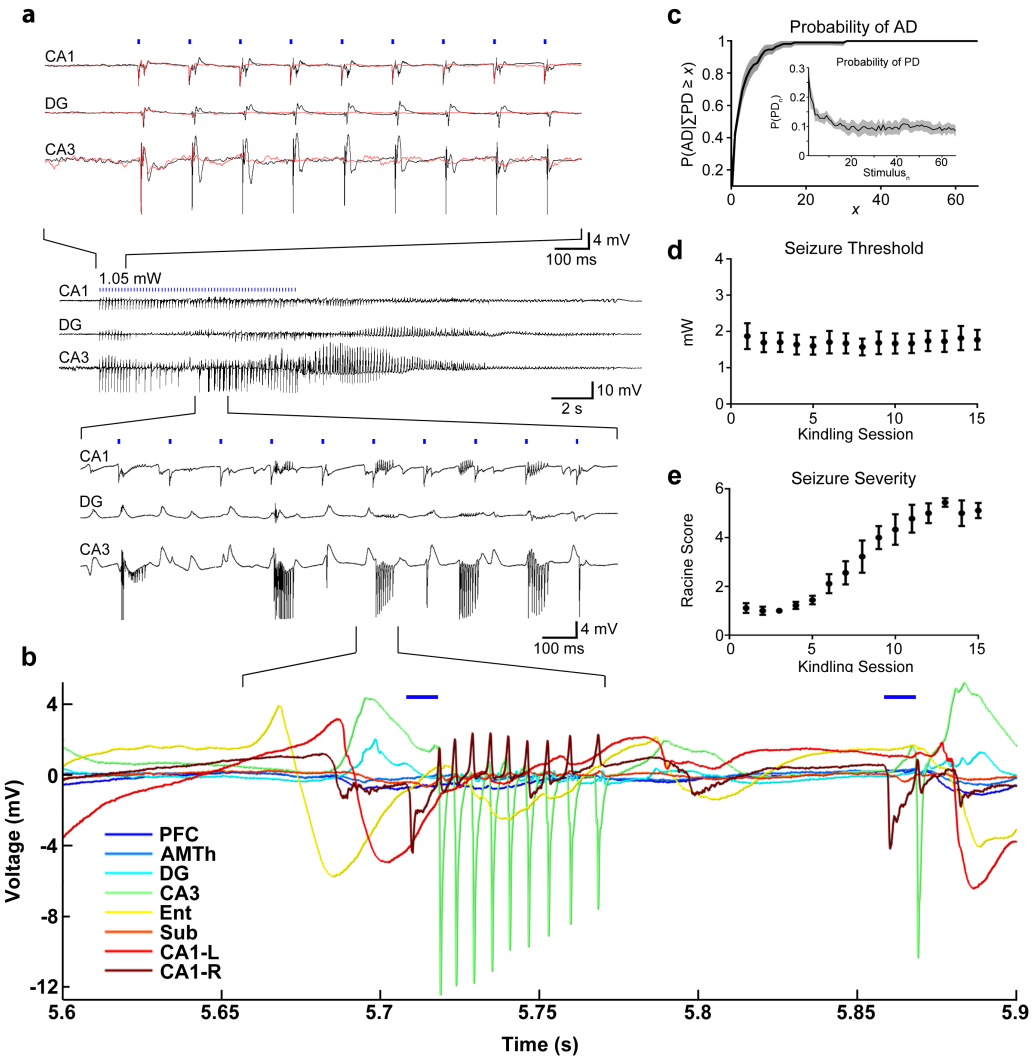

Figure 2 | Optogenetic train stimulation produces an AD. Kindling with daily oADs results in overt behavioral seizure. (**a**) Representative example of an optically-evoked AD. Inset Top: Suprathreshold stimulation levels (for AD) produce network wide PDs (black traces). At subthreshold intensity levels, activation was observed only at the stimulation site (CA1-R), red traces. (**b**) oADs involve high frequency oscillations or epileptiform bursts across multiple hippocampal recording sites with a non-zero phase lag. (**c**) The probability of AD given at least x PDs occurring during the stimulus train. Inset: The overall probability of a PD on each pulse of the train, including subthreshold stimuli. Probabilities were calculated for each animal and the mean is displayed with 95% CIs, n = 7 animals. (**d**) Seizure threshold remained stable throughout the kindling period. (**e**) Behavioral seizure severity increased with each AD and was correlated with stimulation number.

Opto-Kindling and the Emergence of Behavioral Seizure

Using this thresholding procedure, we took a subset of animals (n=7) through an opto-kindling procedure based on those performed previously with electrical stimulation (Goddard et al., 1969; Racine, 1972b) (**Fig. 2c,d**). Threshold oADs were presented daily for 15 days. Traditional electrical kindling results in reduced thresholds and increased behavioral severity (Racine, 1972b). In contrast, the oAD threshold remained stable (uncorrelated with presentation #) over the course of kindling ($r = 0.0865$, $p = 0.759$, ns, n=7) (**Fig. 2c**), in agreement with previously reported optogenetic seizure thresholds obtained by varying stimulus number (Khoshkhoo et al., 2017). The mean oAD threshold during kindling was 1.99 mW (SD 0.827, 95% CI [1.22- 2.75], n=7). Repeated oAD induction was correlated with increasingly severe behavioral seizures as quantified using a modified Racine scale ($r = 0.963$, $p < 0.0001$, n= 7) (**Fig. 2d**). Animals progressed to stage 5 seizures after 9.6 days (SD 2.4, 95% CI [7.4-12], n = 7), considerably faster than corneal or hippocampal kindled mice (Rowley and White, 2010; Stover et al., 2017), but slower than kindling of piriform cortex (McIntyre et al., 1993). The stereotypical behavioral expression (semiology) of the seizure was similar to that observed with electrical kindling (Kairiss et al., 1984; Racine et al., 1972).

oPD Induction and Threshold Measurement

Given the close relationship between the appearance of multiple network wide oPDs following stimulation and subsequent oADs, we sought to determine if the oPD itself was a sufficient indicator of the oADT and therefore, a potential measure of oAD threshold without the need for oAD induction.

Single pulse optogenetic stimulation of CA1 at a sufficient intensity (mean 2.85 mW, SD 0.248, 95% CI [2.34-3.36], n = 30 mice) produced nearly synchronous PDs across the hippocampal and perihippocampal network (**Fig. 3a,b**). The largest amplitude responses were observed in DG and CA3, as well as contralateral CA1. These unitary oPDs closely resembled those induced in the first few pulses of the optical stimulus train used in the oADT procedure, as well as spontaneous discharges (resembling type-2 IIS) observed in AD exposed animals (**Fig. 3a**).

In order to precisely measure the oPDT, we developed a novel optogenetic intensity-response curve procedure that takes advantage of the all or none transition between the sub and suprathreshold response at recording sites downstream of the optogenetic stimulation to accurately detect the occurrence of oPDs (**Fig. 3**). Repeated presentation

of the intensity-response curve revealed considerable variability in the response (oPD vs. no oPD) given a particular stimulus intensity (**Fig. 3 c, d**). However, we found analyzing the probability of an oPD given stimulus intensity x, $P(oPD|I_x)$, allowed for a more robust estimation of threshold.

To generate the oPD probability curve we used twenty intensity levels presented in repeated blocks. Stimuli were presented in random order without replacement so that each stimulus intensity level was presented once per block. Stimulus order was independently randomized for each block. oPD probability was then estimated using multiple replications of stimulus blocks. The intensity levels were selected to linearize the optogenetic response as measured by the mean amplitude of the first peak at the stimulation site, likely a reflection of the ChR2 mediated current and dendritic voltage-gated Na^+ currents (**Fig. 3a-d**).

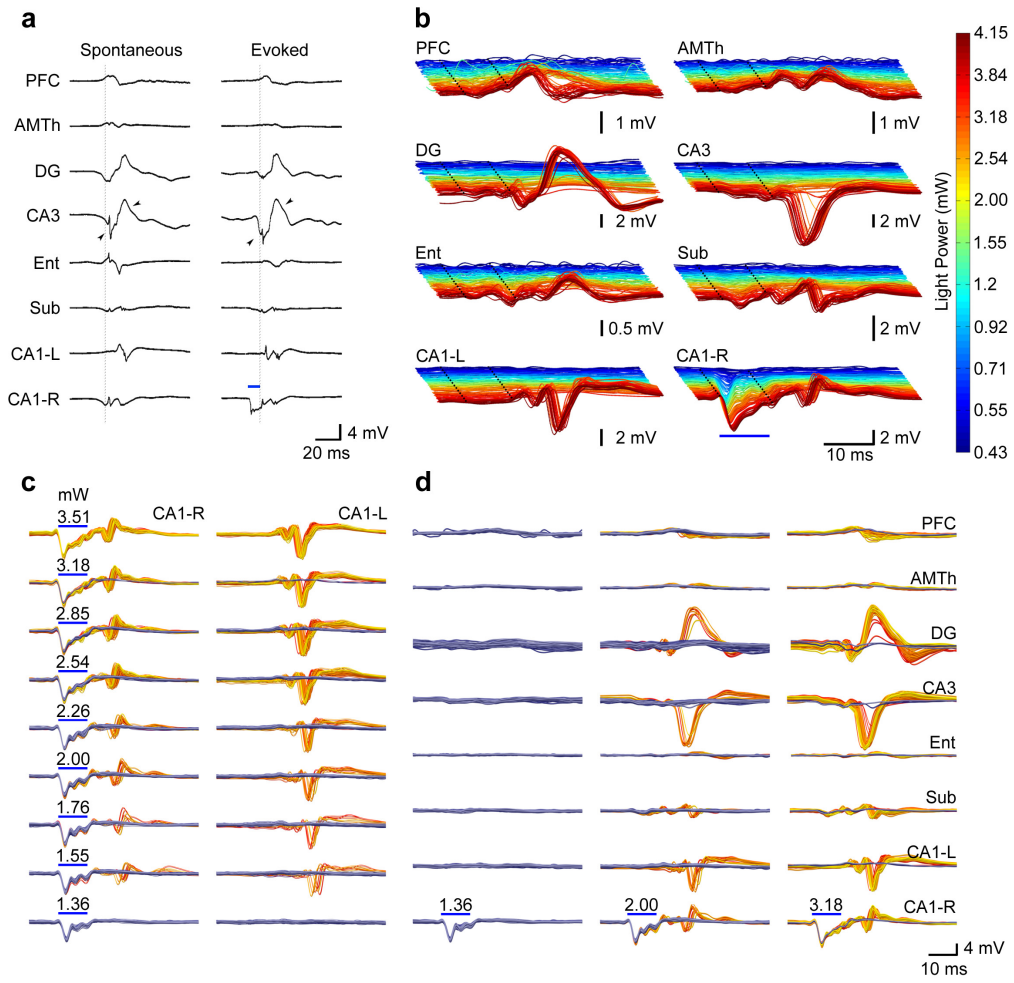

Figure 3 | Optogenetic stimulation produces network wide PDs that closely resemble spontaneous IIS with a probability that increases with light intensity. (**a**) Example comparing spontaneous IIS to oPDs. Spontaneous spikes are characterized by near synchronous activation in DG, CA3, and CA1-R, and delayed activation in CA1-L. Evoked spikes are led by activation in CA1 (stimulation site) followed by near synchronous activation of DG, CA3, and CA1 with a latency of ~10 ms. Note similar timing and wave shape between stimulus evoked spikes and spontaneous spikes (arrow heads). Blue bars indicate onset and duration of light stimulus in CA1. Inter-stimulus interval (ISI) = 3s (**b**) Evoked network activity produced by optogenetic stimulation of area CA1 (right side) at varying light intensities in a representative animal (different from that depicted in **a**). Note large amplitude oPDs evoked at higher intensities. Dotted lines indicate the beginning and end of the light pulse. **(c-d)** Probability of oPD occurrence in downstream sites, rather than amplitude, increases with light intensity at the stimulation site. In area CA1-L, a longer latency response is accompanied by a high amplitude PD. The gold colored traces are those in which a PD was detected, the blue are traces where it was absent. Each plot is an overlay of 60 trials and the color gradient indicates chronological order (dark blue/red for early trials, light blue/yellow for late trials). oPD occurrences: 0/60 @ 1.36 mW, 11/60 @ 2 mW, 58/60 @ 3.18 mW. ISI = 3s. Scale bars in **d** also apply to **c**.

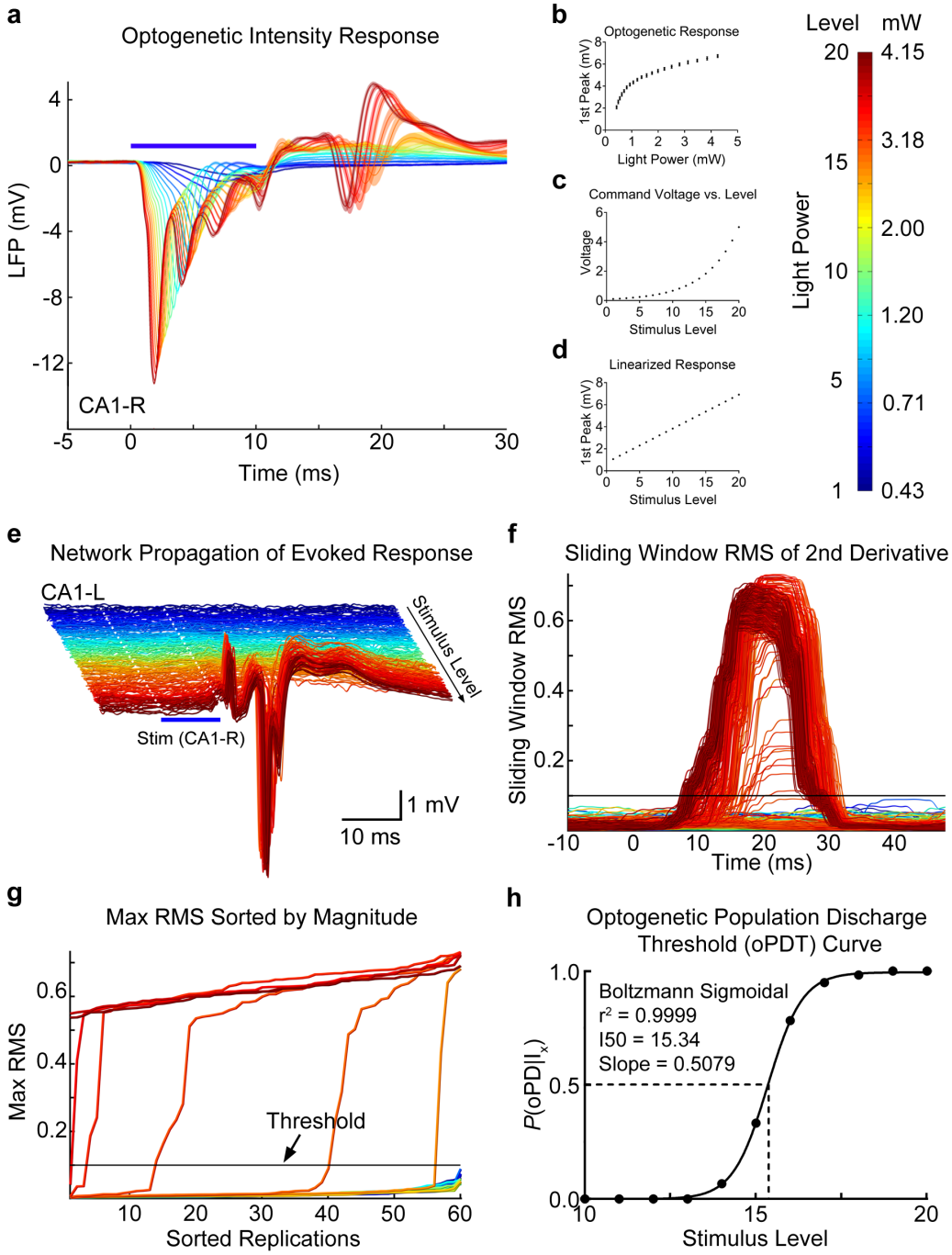

Figure 4 | Summary of the oPDT procedure. (**a**) Average LFP response to optogenetic activation in CA1 at varying light intensities. Shaded bars = 95% confidence intervals. (**b**) The short latency LFP response was used as an approximation of ChR2 mediated current to generate a light intensity-response curve. Mean and SD are displayed. (**c**) A series of light intensities was chosen to produce a linearized optogenetic response **d**. (**e**) The network propagation of evoked activity from the stimulation site (CA1-R, blue bar) to CA1-L. Individual replicates plotted as bandpass filtered (5-300Hz) traces. Colors correspond to the level of the light stimulus (shown in mW on colorbar). 20 levels x 60 replicates = 1200 total stimuli. ISI = 3s. Note high amplitude PDs. (**f**) Sliding window RMS of the 2nd derivative calculated from **e**. Horizontal line indicates the threshold. (**g**) Max RMS (within time window) for each light level sorted by magnitude. Threshold is set in the steep part of the curve. (**h**) oPD ratio (oPDs/total stimuli) plot fit by the Boltzmann sigmoid allows for calculation of an I50, or the LED power at which 50% of the stimuli produce a oPD.

Network oPDs were detected by thresholding a sliding window root-mean-square (RMS) of the 2nd derivative of the peri-stimulus activity (**Fig. 3e-g**). The oPD occurs across the network, and therefore, any channel or combination of channels can be used for oPD detection, including the long latency response at the stimulation site; however, we found that contralateral CA1 provided the greatest separation between sub- and suprathreshold responses. The sub-supra separation was visualized by plotting the sorted peak values of the RMS for each level (**Fig. 3g**). Good separation produces a steep transition with few intermediate values. This plot is also useful for setting the threshold and the

steepness of the transition reduces the detection bias introduced by threshold selection. As a result, the oPDT curve is robust to any choice of threshold within the steep transition region of the sorted peak RMS plot.

Once oPDs have been detected, the proportion of oPDs to total stimulus presentations at each level can then be plotted to generate an oPD threshold curve (oPDT). We then fit the data with the Hodgkin and Huxley formulation of the Boltzmann distribution and calculated the I50, or the intensity at which the probability of oPD was 50% (Hodgkin and Huxley, 1952)(**Fig. 4h**). Expressing the I50 in the arbitrary linearized scale (1-20 levels) is convenient for making comparisons, however, it can easily be converted into power (mW) or irradiance (mW/mm^2) (**Fig. 4b-d**). Using an arbitrary scale and baseline normalization allows for comparisons between animals even when the relationship between power output and optogenetic response vary. In our experience, the variability in baseline I50 between animals, SD = 3.41 levels (n = 20 animals), was larger than the mean I50 variability within animals, mean SD = 1.10 levels, (n = 3-10 baselines per animal). Since ChR2 expression patterns are preserved between animals, it is likely that between animal differences are due to variations in the surgical preparation and the transmission efficiency of the implanted fiber.

Relationship between the oPDT and oADT

Our analysis of the oADT, above, revealed that multiple oPDs must be evoked by the train stimulus in order to generate an AD (**Fig. 2c**). This suggests that the oADT is actually the oPDT, in terms of light intensity. We compared the oADT and the oPDT measured in the same animals using the same chronically implanted fiber. We found that the oADT was correlated with pre-kindling I50 across animals with a slope approaching 1 (1st Seizure: Lin. Reg. Slope: 1.05, 95% CI [0.677, 1.42], Pearson's r = 0.956, p = 0.00078, *n* = 7; Avg Seizure: Lin. Reg. Slope: 0.830, 95% CI [0.462, 1.20], Pearson's r = 0.933, p = 0.0021, n = 7) (**Fig. 5a**). This finding combined with the fact that train stimuli subthreshold for the oPD also failed to produce an oAD, indicate that the oPDT and the oADT are equivalent in terms of light intensity delivered from the same implanted fiber, because both require the oPD.

Changes in Excitability Shift the oPD Curve

To test the hypothesis that the $P(oPD|I_x)$ changes with the balance of excitation and inhibition, we used a well-known chemoconvulsant drug, pentylenetetrazol (PTZ), in non-kindled animals. Despite its ability to induce acute seizures, PTZ does not produce a shift in the electrical AD threshold (Karler et al., 1989).

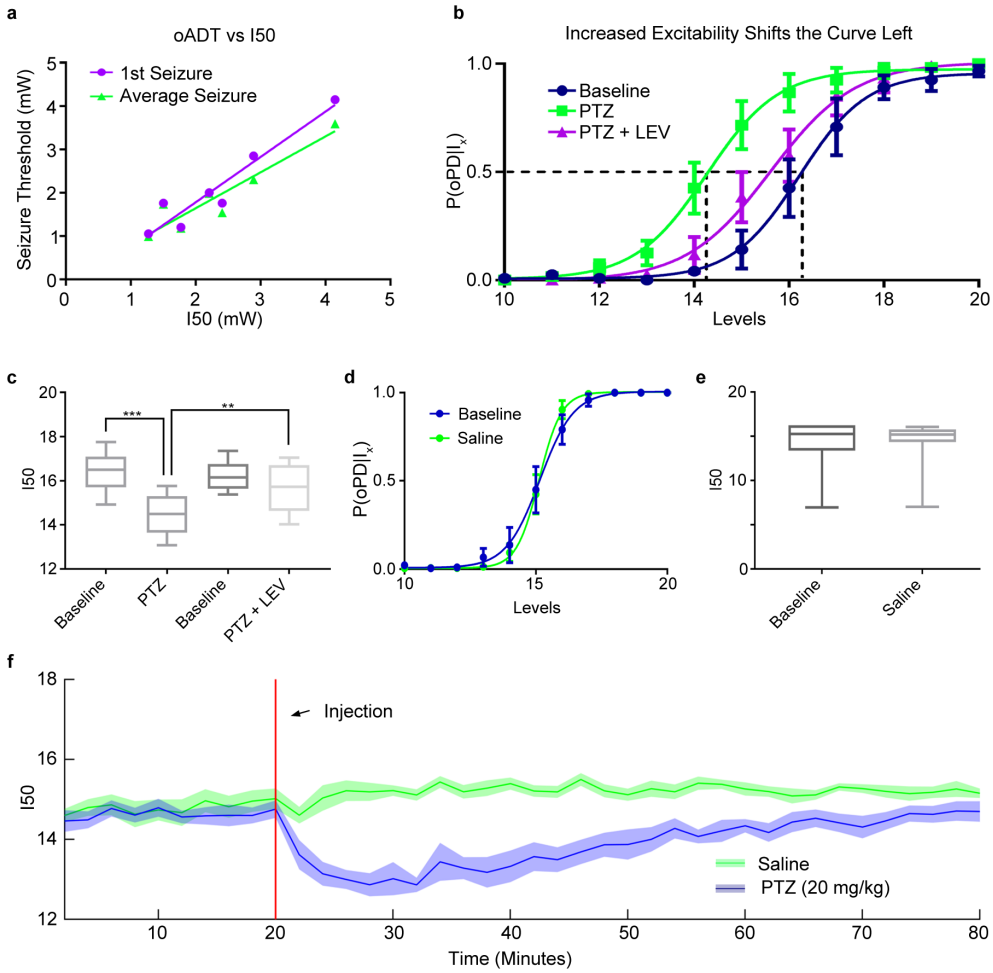

Figure 5 | The I50 is sensitive to changes in network excitability. (**a**) The relationship between pre-seizure I50 and the 1st oADT (purple) or the average oADT throughout 15 kindling sessions (green). (**b,c**) The GABAa antagonist PTZ (20 mg/kg) shifts the oPD curve leftward and treatment with the anticonvulsant drug levetiracetam (40 mg/kg) partially reverses the shift. n = 6 animals. *** p = 0.00043, ** p = 0.0034. (**d,e**) Handling and IP saline administration did not significantly shift the oPD curve compared to baseline (paired t-test, n = 7). (**f**) I50 measurements reveal the time course of PTZ-induced hyperexcitability (disinhibition). Plot of the I50 over time. 6 block bins, n = 9 presentations of each condition (3 trials x 3 animals). Shaded area is mean ± 95% CI.

In contrast, the oPDT was sensitive to PTZ at sub-convulsive doses (20 mg/kg). The I50 was significantly shifted to the left relative to baseline (Baseline = 16.4 levels, SD 0.943, 95% CI [15.4, 17.4], PTZ = 14.5 levels, SD 0.949, 95% CI [13.5, 15.5], p = 0.00041, *n* = 6) (**Fig. 5a,b**), which indicated a reduction in threshold. Although the antiepileptic drug levetiracetam (LEV) failed to show efficacy in the traditional MES and s.c. PTZ acute seizure models (Löscher, 2011), pre-treatment with LEV(40 mg/kg) partially reversed the leftward shift produced by subthreshold PTZ and returned threshold to near baseline levels (PTZ+LEV = 15.7 levels, SD 1.11, 95% CI [14.5, 16.8]) (Baseline vs. PTZ, p = 0.00043, Baseline vs PTZ+LEV, p = 0.12, PTZ vs. PTZ+LEV, p = 0.0034, *n* = 6 repeated-measures ANOVA with Tukey's correction for multiple comparisons) (**Fig.5a,b**). Saline injection did not significantly shift the curve (Baseline vs. Saline, p = 0.99, *n* = 7, paired t-test).

By breaking the stimulus period into bins of presentation blocks, $P(oPD|I_x)$ can be measured over time. Administration of subthreshold PTZ (i.p.) produced a rapid shift in excitability that recovered by about 40 min post-injection (**Fig. 5f**), compared to saline, consistent with the pharmacokinetic curve of PTZ (Yonekawa et al., 1980). For this

example, 6 block bins were used to estimate the I50 at 2 min intervals (6 blocks x 20 stimuli per block x 1s ISI = 120s), but higher temporal resolution is possible by decreasing the bin size and/or the number of stimuli per block.

Stability and Reliability of the oPDT

We assessed the reliability of oPDT measurements by analyzing baseline data to assess short- and long-term stability. Two inter-stimulus intervals (1s and 3s) were used to produce intensity-response curves. This allowed for a comparison of the stability of baseline I50 values generated using each protocol, with the caveat that data from different animals were used. Baselines were selected for further analysis if they were collected in naïve animals (pre-kindling, pre-treatment) (*n* = 67 sessions in 13 animals for 1s, *n* = 41 sessions in 17 animals for 3s int).

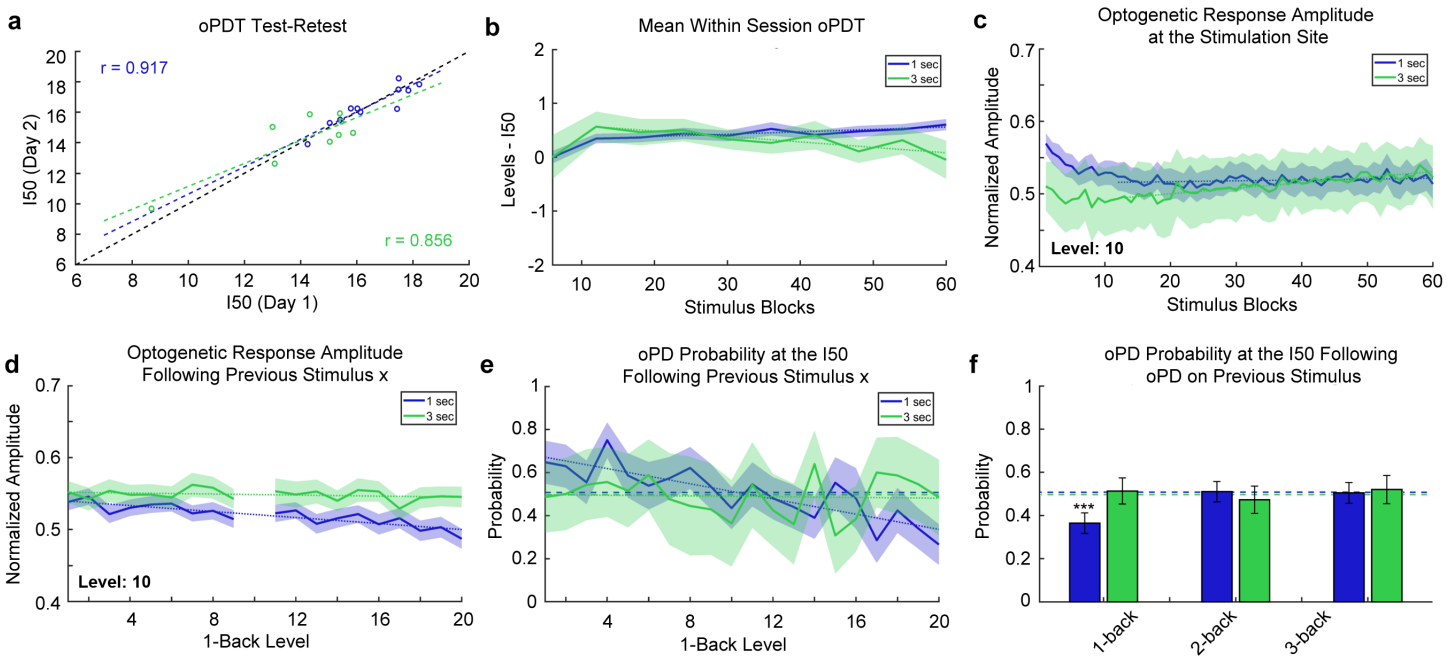

Figure 6 | Stability and Reliability of the oPDT (**a**) Test-retest comparison of session I50s on consecutive days. n = 11 pairs for 1s int and n = 9 pairs for 3s int. Each session I50 is calculated from 60 replicates. Dashed black line indicates the diagonal. (**b**) I50 is relatively stable over the course of a session. Mean normalized intermediate I50s (6 replicate bins) for 1 and 3 sec ISIs. Each stimulus block consisted of 20 intensity levels presented in random order. Order was randomized independently for each block. Session duration is 20 min for the 1s ISI and 60 min for the 3s ISI. n = 67 and 41 sessions for the 1s and 3s ISI respectively. Shaded bars indicate 95% CI. Dotted lines indicate best fit (linear regression) excluding blocks 1-12. (**c**) Optogenetic response amplitude is reduced within the first 5 min of recording, likely due to ChR2 desensitization. Values were transformed via min-max normalization for the entire curve. Same dataset as in **b**. Dotted lines indicate best fit (linear regression) excluding blocks 1-12. (**d**) The optogenetic response amplitude at the stimulation site is reduced following high intensity stimuli. Mean normalized response amplitude at level 10. Same dataset as in **b**. (**e**) The probability of an oPD at the I50 depends on the intensity of the previous stimulus for 1s intervals. Dashed lines indicate the overall probability of an oPD at a level within ±0.25 of the I50. Dotted lines indicate best fit (linear regression). 1s: n = 29 sessions, 1740 trials, 3s: n = 10 sessions, 600 trials. (**f**) oPDs that occur < 2s prior have a suppressive effect on the probability of an oPD at the I50. Dashed lines indicate the overall probability of an oPD at a level within ±0.25 of the I50. Error bars indicate the 95% CI. Same subset as in **e**.

First we looked at the test-retest reliability of measurements (20 levels, 60 replications each) taken on consecutive days (**Fig. 6a).** The measured I50s were consistently reliable with an overall correlation coefficient > 0.85 (1s int: r = 0.917, 95% CI [0.705, 0.979], p < 0.0001, *n* = 11 pairs, 3s int: r = 0.856, 95% CI [0.446, 0.969], p = 0.0032, *n* = 9 pairs, Pearson's).

Mono-synaptic stimulation of CA1 afferents at 1 s intervals has been shown to induce long-term depression (LTD) in vivo (Thiels et al., 1994; Oliet et al., 1997; Massey and Bashir, 2007). In order to determine if the multi-synaptic I50 was drifting over time in our preparation, we broke each 60-block session into 10 x 6-block bins and calculated intermediate I50 values normalized by subtracting the overall session I50 (**Fig. 6b**). Following a transient increase for both, session I50 values gradually increased for the 1s interval and decreased for 3s interval (1s int: slope greater than zero, slope: 0.00442 [0.00206, 0.00678], p = 0.0031, 3s int: slope less than zero slope: -0.0101 [-0.0158, -0.00441], p = 0.0040, linear regression of the means excluding the first 12 replicates). This gradual shift in the I50 through time could be a result of plasticity in the network but also ChR2 desensitization at the stimulation site. All ChR variants exhibit desensitization with varying degrees of reduction in peak photocurrents following repeated activation (Lin, 2010; Williams et al., 2013). We checked for ChR2 desensitization by measuring the peak amplitude (session min/max normalized) of the optogenetic response at the stimulation site over time (**Fig. 6c**). We found that the response amplitude is reduced (3%) within the first 4 minutes, likely an effect of desensitization, after which it increased slightly (1s int: slope greater than zero, slope: 1.16×10^{-4}, 95% CI [7.62×10^{-6}, 2.25×10^{-4}], p = 0.037, 3s int: slope greater than zero, slope: 7.63×10^{-4}, 95% CI [6.52×10^{-4}, 8.75×10^{-4}], p<0.0001, linear regression of the means excluding the first 12 replicates). Overall, the baseline drift in the response amplitude and the I50 over time was small relative to the effects of subthreshold PTZ, for instance (**Fig. 5b,f**). Nevertheless, drift must be accounted for in the interpretation of experimental results and all results should be compared to a vehicle control (**Fig. 5e,f**).

Next, we examined possible short term effects of stimulation on the $P(oPD|I_x)$ and assessed trial independence. The extent of ChR2 desensitization depends on the strength of previous activation and higher intensity stimuli are expected to produce greater desensitization than lower intensity stimuli. Since the stimuli are presented in random order, we were able to quantify this effect by measuring the extent of desensitization produced by each stimulus pair. We measured the peak amplitude of the response to a stimulus (level 10) following each of the other stimulus levels (**Fig. 6d**). There was a small reduction in amplitude of the response for strong preceding stimuli (1s int: slope less than

zero, slope: -0.00208, 95% CI [-0.00271, -0.00145], p<0.0001, 3s int: slope not different from zero, slope: -3.58×10^{-4}, 95% CI [-9.56×10^{-4}, 2.40×10^{-4}] p = 0.22, ns, linear regression of the means). In order to determine if this change in amplitude translated into a shift in the oPD probability, we calculated the oPDT probability at or near the I50 for each preceding stimulus (**Fig. 6e**). A subset of the data was selected for this analysis restricted to those sessions with I50 values that were near a presented stimulus level (within ± 0.25 levels of a whole number) (1s: *n* = 29 sessions, 1740 trials, 3s: *n* = 10 sessions, 600 trials). This allowed us to determine if deviations from chance were related to the stimulus order. The probability of oPD was negatively associated with the intensity of the previous stimulus for the 1s but not 3s interval (1s int: slope less than zero, slope: -0.0177, 95% CI [-0.0232, -0.0121], p<0.0001, 3s int: slope not different from zero, slope: -8.37×10^{-4} 95% CI [-0.008, 0.007], p = 0.82). This suggests that the reduction in amplitude (**Fig. 6d**) translates into a reduction in oPD probability.

Higher intensity stimuli are also more likely to produce an oPD, so we checked for effects of the oPD itself on the oPD probability at the I50. We calculated the conditional probability of an oPD at stimulus levels within ± 0.25 of the I50 (where the probability of an oPD should be close to chance), given an oPD on the nth previous stimulus (any level). Each n-back probability was calculated independently. We found a strong suppressive effect of a previous PD for the 1-back stimulus with a 1s ISI compared to the overall probability of an oPD at the I50 (p<0.0001, Fisher's Exact Test, corrected for multiple comparisons using the Holm-Sidak method). PD probability did not differ significantly from chance at 2 and 3 back for the 1s interval (p = 0.91 and 0.32 respectively, Fisher's Exact Test, corrected). PD probability remained at chance for 1, 2, and 3-back for the 3s interval (p = 0.91, 0.51, 0.45 respectively, Fisher's Exact Test, corrected). Therefore, an interval of >2s is expected to be sufficient to produce independent trials (a condition for hypothesis testing using the binomial distribution) and the 1s interval is expected to produce I50s that slightly overestimate the oPDT, likely due to a combination of ChR2 desensitization and after-hyperpolarization produced by the oPD. For this reason, it is important to compare measurements to baselines collected using the same protocol with the same ISI. It is important to note that all of the above measurements were taken from awake behaving animals and include random variation due to changes in ongoing activity. Taken together, these results indicate that the oPDT curve offers exceptional precision and reliability and as such provides a new clear window into the excitability state of the intact brain.

Discussion

Using a novel light intensity-response procedure, we developed and validated a new quantitative measure of network excitability based on PD probability. This approach, the oPDT, has several important features: first, combining optogenetic modulators with a high precision LED light source allows for tighter control over induced currents in specific cells than previously possible with electrical stimulation; second, our multi-site recording technique allows us to simultaneously induce and monitor the propagation of epileptiform activity in behaving animals; third, our chronic preparation permits tracking of excitability over time in response to experimental manipulation; and finally, because the oPDT I50 appears to be a useful measure of excitability, without the need for seizure induction, multiple pharmacological or molecular interventions can be tested within subjects, greatly increasing the ability to detect functional changes as a result of genetic and/or pharmacological manipulation.

Previously seizure thresholds have been determined optogenetically by varying the number of stimulus bouts (Khoshkhoo 2017). The oADT represents the first example of systematic optogenetic intensity-response curves, using a high-precision LED, to precisely determine seizure thresholds (keeping stimulation frequency, pulse width, and train duration constant). By using a multi-site approach, the oPDT is the first technique to determine network discharge thresholds using a probabilistic model to fit intensity-response curves.

The Thy1-ChR2 mice (line 18) used in these experiments express high levels of wild-type ChR2-EYFP in deep (calbindin-negative) pyramidal neurons in CA1 (Arenkiel et al., 2007; Dobbins et al., 2018). Importantly, transgenic animals provide more consistent and specific ChR2 expression patterns than could be achieved with virus injection. Compared to neighboring superficial cells, deep pyramidal neurons in CA1 are more prone to burst firing, have unique input and output pathways, and lack calcium buffering proteins, potentially making them more susceptible to seizure activity (Mizuseki et al., 2011; Sloviter, 1989; Valero et al., 2015). By selectively targeting this population of excitatory neurons the inhibitory population is free to respond, which preserves the strong reciprocal relationship they have with the excitatory cells being stimulated and allows them to participate in the generation of the synchronous discharge (Cobb et al., 1995; Ellender et al., 2014; Sessolo et al., 2015; Yekhlef et al., 2015; Khoshkhoo et al., 2017; Wang et al., 2017; Chang et al., 2018a).

Electrical stimulation activates cells and fibers of passage which act upon a sparse and widely distributed population of neurons whose identity cannot be predicted ahead of time, nor known with certainty afterwards (Histed et al., 2009). In contrast, optogenetic expression patterns can readily be determined histologically and light spread can be accurately modeled based on fiber location and power output. Light spreads out in a cone from the tip of the fiber and drops off quickly with distance in brain tissue due to scattering (Aravanis et al., 2007; Yizhar et al., 2011). ChR2 is strongly expressed in both the basal and apical dendrites of CA1 pyramidal neurons. As a general rule, dendrites are much more excitable than axons or the cell body due to increased surface area (Huber et al., 2008). As the light intensity increases, cells directly under the fiber will be increasingly depolarized to threshold followed by neighboring cells. Thus, the optogenetic intensity-response curve varies both the magnitude of depolarization in individual cells as well as the overall size of the activated population. Cells in the center that have already reached threshold cannot be depolarized further, in part because ChR2 currents are voltage dependent (Williams et al., 2013). Depending on the pulse duration, cells held in a depolarized state will fire bursts instead of single action potentials (Boyden et al., 2005). From the perspective of downstream areas, the intensity-response curve varies the number of synchronously active projections emanating from the stimulation site.

As a result of the enhanced precision and reliability of the oPDT, it has a number of important advantages compared to commonly used seizure models. The maximal electric shock and PTZ seizure models have been the mainstay of anti-convulsant drug screens for many years (Löscher, 2011). MES and PTZ use increasing electrical current or convulsant dosage, respectively, to determine a seizure threshold, similar to the light intensity-response curves used in the oPDT. Unlike the MES and PTZ models, the oPDT and oADT uses an unambiguous physiological distinction between normal and abnormal activity, avoiding the need for subjective judgments of seizure behavior. This also alleviates the need for the induced seizure to involve motor cortex (in order to produce behavioral seizure), potentially making it a better model of complex partial seizures which may not have a motor component (D'Ambrosio and Miller, 2010). Unlike the oADT, the oPDT represents a novel metric of excitability because it measures PD thresholds rather than seizure thresholds. Although the thresholds for both metrics are the same in terms of light intensity, the oADT requires repeated oPD inductions in order to produce an AD. This suggests that distinct mechanisms are involved in the oAD generation, such as the accumulation of extracellular K+ and the switch to depolarizing GABA (Alfonsa et al., 2015;

Buchin et al., 2016; Cossart et al., 2005; Miles et al., 2012). Comparing the results of each approach might allow for identification of drugs and manipulations that prevent AD but do not change baseline excitability, and therefore have fewer side effects. The oPDT directly measures the probability of oPD given a particular light intensity within each subject and as such is a more sensitive measurement of threshold that takes variability due to ongoing activity into account. This property allows for measurements of smaller changes with fewer animals, offsetting the additional difficulty of the surgical preparation and the need for transgenic mice.

The failure of the electrical ADT to detect the pro-convulsive effects of PTZ and the anti-epileptic properties of levetiracetam (Löscher, 2011) suggests that electrical stimulation, by injecting current into the local extracellular space, produces an AD that is not sensitive to the balance of excitation and inhibition, or synaptic efficacy. This fact limits its utility in assessing seizure susceptibility because it likely bypasses these important regulators of network excitability. The oPDT on the other hand, seems to be a more sensitive measure of factors such as these that regulate the probability of synchronous discharge.

Electrically evoked potential amplitude has previously been used as a measure of excitability in animal models and patients with epilepsy (Maru and Goddard, 1987; Freestone et al., 2011; Enatsu et al., 2012; Wendling et al., 2016; Keller et al., 2018). However, without knowing the details of underlying synaptic currents and their influence on the LFP, it is difficult to estimate excitability from amplitude alone given that somatic inhibition and dendritic excitation produce similar sink/source patterns (Buzsáki et al., 2012; Hales and Pockett, 2014; Herreras, 2016). Because network wide PDs are readily differentiated from subthreshold synaptic potentials, our preparation provides an unambiguous measurement of excitability that does not require knowledge of the sink/source patterns needed to interpret the LFP itself.

The sharp transition between sub and suprathreshold activity may reflect a breakdown between the balance of feedforward inhibition and excitation (Buzsáki, 1984; Wahlstrom-Helgren and Klyachko, 2016). If the magnitude of the population EPSP exceeds that of feedforward inhibition, it could produce a highly synchronous discharge that would propagate to other areas (Johnston and Brown, 1981). This would explain the sensitivity of the oPDT curve to GABA antagonists such as PTZ. In addition to the balance of inhibition and excitation, a number of other functional properties might be expected to modulate the oPDT, the oADT, or both. Synaptic strength determines the threshold for

downstream propagation of the synchronous discharge (Nicoll, 2017), intrinsic excitability modulates the responsiveness of downstream cells, which is governed by the relative expression and cellular localization of voltage-gated Na^+, K^+, and Ca^{2+} channels (Graef and Godwin, 2010; Lisman et al., 2018; Meadows et al., 2016), and also by the extracellular space and its regulation by glia (Devinsky et al., 2013).

The fact that the evoked discharges initiated in CA1 occurred simultaneously in multiple hippocampal structures supports the hypothesis that synchronous activation of entorhinal cortex was responsible (Avoli et al., 2002; Yeckel and Berger, 1990). The oPD was most prominent in areas CA3 and DG; reciprocally connected areas prone to hypersynchronous discharge (Traub and Jefferys, 1994). CA3 and DG lead during spontaneous discharges suggesting that synchronous inputs to these areas are responsible for generating the IIS, and optogenetically generated synchronous input from CA1 via subiculum and entorhinal cortex serves as a trigger for the oPD. These results are also consistent with the dentate gate hypothesis, which posits that dentate granule cells, because of their relatively high functional threshold, act as a gate that prevents the propagation of seizure activity into the rest of hippocampus (Heinemann et al., 1992; Lothman et al., 1992; Goldberg and Coulter, 2013). Although hippocampus has multiple interacting nested loops, if the dentate gyrus is the last to reach "critical mass", a synchronous discharge there could be responsible for the all-or-none expression of the oPD. It this is true, the oPDT, in its current configuration, is a sensitive measure of the strength of the "dentate gate" and could be useful for evaluating therapeutic interventions in this area (Krook-Magnuson et al., 2013, 2015). Non-synaptic propagation, often neglected in earlier studies of seizure, is also likely to play a role in generating the synchronous discharge in the closely situated structures of the hippocampus (Zhang et al., 2014).

Despite the widespread synchronous nature of the discharge, it is transient, and the system is surprisingly resilient to its effects on short time scales. By analyzing the oPD probabilities from one stimulus to the next, we found that the response is functionally independent of the previous stimulus in just a few seconds. Furthermore, closely spaced oPDs (1s ISI) are suppressive to the system, significantly reducing the probability of another oPD in response to the subsequent stimulus. The suppressive effect of the oPD is likely due to a combination of ChR2 desensitization and the slow after-hyperpolarization (I_{sAHP}) (Alger and Nicoll, 1980; Lancaster and Adams, 1986). The fact that unitary PDs are suppressive and multiple repeated oPDs are required to initiate seizure suggests that either there is a reduction in the suppressive effect with each oPD, or that multiple PDs produce sufficient excitation to overcome the suppressive

effects. In the context of spontaneous seizure, this makes it clear that seizures are a result of a slow transition to abnormal brain states, such as those presumably induced by persistence repetitive synchronous discharges in our model, which are permissive to self-sustaining seizure activity and that they are not simply the result of transient synchronous activity alone (Chang et al., 2018b).

The oPDT procedure allows for multiple threshold measurements over time; an important advantage over previous methods. For comparison, the recovery time for the 6hz – psychomotor seizure and minimal electroshock threshold is at least 4.4 and 7.5 minutes respectively (Brown et al., 1953). The enhanced temporal resolution of the oPDT can be used to estimate the functional pharmacokinetics of anti-epileptic drugs or to study the natural fluctuations in excitability that depend on brain state and behavior (Baud et al., 2018, 2019). The temporal resolution of the oPDT is limited by the number of stimuli used to generate the curve and the ISI. As we have demonstrated, stimuli are functionally independent when presented with ISI > 2s. Further reductions could be achieved by using a reduced subset of stimuli, optimized for baseline curves in each animal. For small changes, sampling at the I50 alone should be sufficient. When implemented in a closed-loop system, optimization techniques could be used to further reduce the number of stimuli necessary (MacKay, 1992). It may also be possible to use the oPDT as a measure of excitability over time in models of epileptogenesis as a way to gain insight into mechanisms and measure the effectiveness of various pharmacological and molecular interventions. Finally, because the oPDT provides a quantitative measure of excitability, it is well suited to measurement of the relative efficacy (rather than just the potency) of anti-epileptic drugs (Löscher, 2011).

On longer time scales (days to weeks), repeated stimulation of brain is expected to produce a number of changes to the system, some of which involve changes in plasticity and homeostatic regulation of the stimulated cells (Thiels et al., 1994; Oliet et al., 1997; Massey and Bashir, 2007). Recently, it was demonstrated that long-term (24hrs) optogenetic stimulation of CA1 produces changes in spine density and synaptic plasticity (Moulin et al., 2019). Although we have demonstrated that the oPDT is stable over time, appropriate control experiments should be used and care should be taken when interpreting results to account for potential changes in the brain as a result of stimulation.

The current study is focused on using optogenetic intensity-response curves to quantify excitability in the context of seizure activity, but the same procedure could be applied to any study that uses optogenetic stimulation as

the independent variable with a stochastic dependent variable. Similar procedures could be performed with any appropriate optogenetically induced cellular, molecular, physiological, or behavioral output metric (Allen et al., 2015; Bugaj et al., 2016; Tischer and Weiner, 2014). Abnormal excitability is also associated with a number of other neurological disorders including depression, autism, Alzheimer's, anxiety, drug addiction (and withdrawal), and schizophrenia (Crabtree et al., 2017; Friedman et al., 2014; Kourrich et al., 2015; Rau et al., 2015; Santos et al., 2010; Takarae and Sweeney, 2017). Correlating changes in excitability with behavior or neurochemical state in the context of these disorders may provide novel insights into the mechanisms of the underlying disease.

Synchronous optogenetic activation is sufficient to induce epileptiform population discharges and the systematic modulation of light intensity allows for quantitative estimation of the threshold between normal and abnormal activity. This approach has the potential to provide important insights into the relationship between epileptiform spikes and seizure and provides a novel platform for testing the effects of therapeutic interventions on network excitability.

Acknowledgements

Special thanks to: Dorothy Dobbins, Rasesh Joshi, Allison Goldstein, Hong Qu Shan, and Glen Marrs for help with this project. Funding was provided by the NIH grants R01AA016852, T32AA007565, F31AA021322, and the Tab Williams Family Fund. Portions of this work were previously reported in abstract form (Klorig et al., 2014, 2017).

Contributions

DK and GA designed experiments and performed surgeries. DK, GA, and TS collected data. DK developed the analysis. DK, DG, and GA wrote the paper.

References

Alfonsa, H., Merricks, E.M., Codadu, N.K., Cunningham, M.O., Deisseroth, K., Racca, C., and Trevelyan, A.J. (2015). The contribution of raised intraneuronal chloride to epileptic network activity. J. Neurosci. Off. J. Soc. Neurosci. *35*, 7715–7726.

Alger, B.E., and Nicoll, R.A. (1980). Epileptiform burst afterhyperolarization: calcium-dependent potassium potential in hippocampal CA1 pyramidal cells. Science *210*, 1122–1124.

Allen, B.D., Singer, A.C., and Boyden, E.S. (2015). Principles of designing interpretable optogenetic behavior experiments. Learn. Mem. *22*, 232–238.

Aravanis, A.M., Wang, L.P., Zhang, F., Meltzer, L.A., Mogri, M.Z., Schneider, M.B., and Deisseroth, K. (2007). An optical neural interface: in vivo control of rodent motor cortex with integrated fiberoptic and optogenetic technology. J Neural Eng *4*, S143–S156.

Arenkiel, B.R., Peca, J., Davison, I.G., Feliciano, C., Deisseroth, K., Augustine, G.J., Ehlers, M.D., and Feng, G. (2007). In vivo light-induced activation of neural circuitry in transgenic mice expressing channelrhodopsin-2. Neuron *54*, 205–218.

Avoli, M., D'Antuono, M., Louvel, J., Köhling, R., Biagini, G., Pumain, R., D'Arcangelo, G., and Tancredi, V. (2002). Network and pharmacological mechanisms leading to epileptiform synchronization in the limbic system in vitro. Prog. Neurobiol. *68*, 167–207.

Barton, M.E., Klein, B.D., Wolf, H.H., and White, H.S. (2001). Pharmacological characterization of the 6 Hz psychomotor seizure model of partial epilepsy. Epilepsy Res. *47*, 217–227.

Baud, M.O., Kleen, J.K., Mirro, E.A., Andrechak, J.C., King-Stephens, D., Chang, E.F., and Rao, V.R. (2018). Multi-day rhythms modulate seizure risk in epilepsy. Nat. Commun. *9*, 88.

Baud, M.O., Ghestem, A., Benoliel, J.-J., Becker, C., and Bernard, C. (2019). Endogenous multidien rhythm of epilepsy in rats. Exp. Neurol.

Boyden, E.S., Zhang, F., Bamberg, E., Nagel, G., and Deisseroth, K. (2005). Millisecond-timescale, genetically targeted optical control of neural activity. Nat Neurosci *8*, 1263–1268.

Bragin, A., Csicsvári, J., Penttonen, M., and Buzsáki, G. (1997). Epileptic afterdischarge in the hippocampal-entorhinal system: current source density and unit studies. Neuroscience *76*, 1187–1203.

Bragin, A., Engel, J., Jr, Wilson, C.L., Fried, I., and Mathern, G.W. (1999). Hippocampal and entorhinal cortex high-frequency oscillations (100--500 Hz) in human epileptic brain and in kainic acid--treated rats with chronic seizures. Epilepsia *40*, 127–137.

Bragin, A., Wilson, C.L., and Jr, J.E. (2002). Increased afterdischarge threshold during kindling in epileptic rats. Exp. Brain Res. *144*, 30–37.

Bragin, A., Wilson, C.L., Almajano, J., Mody, I., and Engel, J., Jr (2004). High-frequency oscillations after status epilepticus: epileptogenesis and seizure genesis. Epilepsia *45*, 1017–1023.

Bragin, A., Azizyan, A., Almajano, J., Wilson, C.L., and Engel, J., Jr (2005). Analysis of chronic seizure onsets after intrahippocampal kainic acid injection in freely moving rats. Epilepsia *46*, 1592–1598.

Brown, W.C., Schiffman, D.O., Swinyard, E.A., and Goodman, L.S. (1953). Comparative Assay of Antiepileptic Drugs by "Psychomotor" Seizure Test and Minimal Electroshock Threshold Test. J. Pharmacol. Exp. Ther. *107*, 273–283.

Buchin, A., Chizhov, A., Huberfeld, G., Miles, R., and Gutkin, B.S. (2016). Reduced Efficacy of the KCC2 Cotransporter Promotes Epileptic Oscillations in a Subiculum Network Model. J. Neurosci. Off. J. Soc. Neurosci. *36*, 11619–11633.

Bugaj, L.J., O'Donoghue, G.P., and Lim, W.A. (2016). Interrogating cellular perception and decision making with optogenetic tools. J Cell Biol jcb.201612094.

Buzsáki, G. (1984). Feed-forward inhibition in the hippocampal formation. Prog. Neurobiol. *22*, 131–153.

Buzsáki, G., Anastassiou, C.A., and Koch, C. (2012). The origin of extracellular fields and currents — EEG, ECoG, LFP and spikes. Nat. Rev. Neurosci. *13*, 407.

Cardin, J.A., Carlén, M., Meletis, K., Knoblich, U., Zhang, F., Deisseroth, K., Tsai, L.-H., and Moore, C.I. (2010). Targeted optogenetic stimulation and recording of neurons in vivo using cell-type-specific expression of Channelrhodopsin-2. Nat. Protoc. *5*, 247–254.

Chang, M., Dian, J.A., Dufour, S., Wang, L., Moradi Chameh, H., Ramani, M., Zhang, L., Carlen, P.L., Womelsdorf, T., and Valiante, T.A. (2018a). Brief activation of GABAergic interneurons initiates the transition to ictal events through post-inhibitory rebound excitation. Neurobiol. Dis. *109*, 102–116.

Chang, W.-C., Kudlacek, J., Hlinka, J., Chvojka, J., Hadrava, M., Kumpost, V., Powell, A.D., Janca, R., Maturana, M.I., Karoly, P.J., et al. (2018b). Loss of neuronal network resilience precedes seizures and determines the ictogenic nature of interictal synaptic perturbations. Nat. Neurosci. *21*, 1742.

Cobb, S.R., Buhl, E.H., Halasy, K., Paulsen, O., and Somogyi, P. (1995). Synchronization of neuronal activity in hippocampus by individual GABAergic interneurons. Nature *378*, 75.

Cossart, R., Bernard, C., and Ben-Ari, Y. (2005). Multiple facets of GABAergic neurons and synapses: multiple fates of GABA signalling in epilepsies. Trends Neurosci. *28*, 108–115.

Crabtree, G.W., Sun, Z., Kvajo, M., Broek, J.A.C., Fénelon, K., McKellar, H., Xiao, L., Xu, B., Bahn, S., O'Donnell, J.M., et al. (2017). Alteration of Neuronal Excitability and Short-Term Synaptic Plasticity in the Prefrontal Cortex of a Mouse Model of Mental Illness. J. Neurosci. Off. J. Soc. Neurosci. *37*, 4158–4180.

D'Agostino, R.B., Belanger, A., and D'Agostino, R.B. (1990). A Suggestion for Using Powerful and Informative Tests of Normality. Am. Stat. *44*, 316.

D'Ambrosio, R., and Miller, J.W. (2010). What is an Epileptic Seizure? Unifying Definitions in Clinical Practice and Animal Research to Develop Novel Treatments. Epilepsy Curr. *10*, 61–66.

Devinsky, O., Vezzani, A., Najjar, S., Lanerolle, N.C.D., and Rogawski, M.A. (2013). Glia and epilepsy: excitability and inflammation. Trends Neurosci. *36*, 174–184.

Dobbins, D.L., Klorig, D.C., Smith, T., and Godwin, D.W. (2018). Expression of channelrhodopsin-2 localized within the deep CA1 hippocampal sublayer in the Thy1 line 18 mouse. Brain Res. *1679*, 179–184.

Ellender, T.J., Raimondo, J.V., Irkle, A., Lamsa, K.P., and Akerman, C.J. (2014). Excitatory effects of parvalbumin-expressing interneurons maintain hippocampal epileptiform activity via synchronous afterdischarges. J. Neurosci. Off. J. Soc. Neurosci. *34*, 15208–15222.

Enatsu, R., Piao, Z., O'Connor, T., Horning, K., Mosher, J., Burgess, R., Bingaman, W., and Nair, D. (2012). Cortical excitability varies upon ictal onset patterns in neocortical epilepsy: A cortico-cortical evoked potential study. Clin. Neurophysiol. *123*, 252–260.

Freestone, D.R., Kuhlmann, L., Grayden, D.B., Burkitt, A.N., Lai, A., Nelson, T.S., Vogrin, S., Murphy, M., D'Souza, W., Badawy, R., et al. (2011). Electrical probing of cortical excitability in patients with epilepsy. Epilepsy Behav. *22*, S110–S118.

Friedman, A.K., Walsh, J.J., Juarez, B., Ku, S.M., Chaudhury, D., Wang, J., Li, X., Dietz, D.M., Pan, N., Vialou, V.F., et al. (2014). Enhancing Depression Mechanisms in Midbrain Dopamine Neurons Achieves Homeostatic Resilience. Science *344*, 313–319.

Goddard, G.V., McIntyre, D.C., and Leech, C.K. (1969). A permanent change in brain function resulting from daily electrical stimulation. Exp. Neurol. *25*, 295–330.

Goldberg, E.M., and Coulter, D.A. (2013). Mechanisms of epileptogenesis: a convergence on neural circuit dysfunction. Nat. Rev. Neurosci. *14*, 337–349.

Graef, J.D., and Godwin, D.W. (2010). Intrinsic plasticity in acquired epilepsy: too much of a good thing? The Neuroscientist *16*, 487–495.

Hales, C.G., and Pockett, S. (2014). The relationship between local field potentials (LFPs) and the electromagnetic fields that give rise to them. Front. Syst. Neurosci. *8*.

Heinemann, U., Beck, H., Dreier, J.P., Ficker, E., Stabel, J., and Zhang, C.L. (1992). The dentate gyrus as a regulated gate for the propagation of epileptiform activity. Epilepsy Res. Suppl. *7*, 273–280.

Herreras, O. (2016). Local Field Potentials: Myths and Misunderstandings. Front. Neural Circuits *10*, 101.

Histed, M.H., Bonin, V., and Reid, R.C. (2009). Direct activation of sparse, distributed populations of cortical neurons by electrical microstimulation. Neuron *63*, 508–522.

Hodgkin, A.L., and Huxley, A.F. (1952). A quantitative description of membrane current and its application to conduction and excitation in nerve. J. Physiol. *117*, 500–544.

Huber, D., Petreanu, L., Ghitani, N., Ranade, S., Hromadka, T., Mainen, Z., and Svoboda, K. (2008). Sparse optical microstimulation in barrel cortex drives learned behaviour in freely moving mice. Nature. *451*, 61–64.

Johnston, D., and Brown, T.H. (1981). Giant synaptic potential hypothesis for epileptiform activity. Science *211*, 294–297.

Kairiss, E.W., Racine, R.J., and Smith, G.K. (1984). The development of the interictal spike during kindling in the rat. Brain Res. *322*, 101–110.

Karler, R., Murphy, V., Calder, L.D., and Turkanis, S.A. (1989). Pentylenetetrazol kindling in mice. Neuropharmacology *28*, 775–780.

Keller, C.J., Huang, Y., Herrero, J.L., Fini, M., Du, V., Lado, F.A., Honey, C.J., and Mehta, A.D. (2018). Induction and quantification of excitability changes in human cortical networks. J. Neurosci. 1088–17.

Khoshkhoo, S., Vogt, D., and Sohal, V.S. (2017). Dynamic, Cell-Type-Specific Roles for GABAergic Interneurons in a Mouse Model of Optogenetically Inducible Seizures. Neuron *93*, 291–298.

Klorig, D.C., and Godwin, D.W. (2014). A magnetic rotary optical fiber connector for optogenetic experiments in freely moving animals. J. Neurosci. Methods *227C*, 132–139.

Klorig, D.C., Masicampo, M., Bass, C.E., and Godwin, D.W. (2014). Kindling, High Frequency Oscillations, and Interictal Spikes in an Optogenetic Model of Seizure. Soc Neurosci.

Klorig, D.C., Alberto, G., and Godwin, D.W. (2017). Optogenetically induced population discharge threshold (oPDT) as a sensitive measure of excitability. Soc Neurosci.

Kourrich, S., Calu, D.J., and Bonci, A. (2015). Intrinsic plasticity: an emerging player in addiction. Nat. Rev. Neurosci. *16*, 173–184.

Krook-Magnuson, E., Armstrong, C., Oijala, M., and Soltesz, I. (2013). On-demand optogenetic control of spontaneous seizures in temporal lobe epilepsy. Nat. Commun. *4*, 1376.

Krook-Magnuson, E., Armstrong, C., Bui, A., Lew, S., Oijala, M., and Soltesz, I. (2015). In vivo evaluation of the dentate gate theory in epilepsy. J. Physiol. *593*, 2379–2388.

Lancaster, B., and Adams, P.R. (1986). Calcium-dependent current generating the afterhyperpolarization of hippocampal neurons. J. Neurophysiol. *55*, 1268–1282.

Lévesque, M., and Avoli, M. (2013). The kainic acid model of temporal lobe epilepsy. Neurosci. Biobehav. Rev. *37*, 2887–2899.

Lin, J.Y. (2010). A User's Guide to Channelrhodopsin Variants: Features, Limitations and Future Developments. Exp. Physiol.

Lisman, J., Cooper, K., Sehgal, M., and Silva, A.J. (2018). Memory formation depends on both synapse-specific modifications of synaptic strength and cell-specific increases in excitability. Nat. Neurosci. *21*, 309–314.

Löscher, W. (2011). Critical review of current animal models of seizures and epilepsy used in the discovery and development of new antiepileptic drugs. Seizure *20*, 359–368.

Lothman, E.W., Stringer, J.L., and Bertram, E.H. (1992). The dentate gyrus as a control point for seizures in the hippocampus and beyond. Epilepsy Res. Suppl. *7*, 301–313.

MacKay, D.J.C. (1992). Information-Based Objective Functions for Active Data Selection. Neural Comput. *4*, 590–604.

Maru, E., and Goddard, G.V. (1987). Alteration in dentate neuronal activities associated with perforant path kindling: I. Long-term potentiation of excitatory synaptic transmission. Exp. Neurol. *96*, 19–32.

Massey, P.V., and Bashir, Z.I. (2007). Long-term depression: multiple forms and implications for brain function. Trends Neurosci. *30*, 176–184.

McIntyre, D.C., Kelly, M.E., and Armstrong, J.N. (1993). Kindling in the perirhinal cortex. Brain Res. *615*, 1–6.

Meadows, J.P., Guzman-Karlsson, M.C., Phillips, S., Brown, J.A., Strange, S.K., Sweatt, J.D., and Hablitz, J.J. (2016). Dynamic DNA methylation regulates neuronal intrinsic membrane excitability. Sci Signal *9*, ra83–ra83.

Miles, R., Blaesse, P., Huberfeld, G., Wittner, L., and Kaila, K. (2012). Chloride homeostasis and GABA signaling in temporal lobe epilepsy. In Jasper's Basic Mechanisms of the Epilepsies, J.L. Noebels, M. Avoli, M.A. Rogawski, R.W. Olsen, and A.V. Delgado-Escueta, eds. (Bethesda (MD): National Center for Biotechnology Information (US)), p.

Mizuseki, K., Diba, K., Pastalkova, E., and Buzsáki, G. (2011). Hippocampal CA1 pyramidal cells form functionally distinct sublayers. Nat. Neurosci. *14*, 1174–1181.

Moulin, T.C., Petiz, L.L., Rayêe, D., Winne, J., Maia, R.G., Cruz, R.V.L. da, Amaral, O.B., and Leão, R.N. (2019). Chronic in vivo optogenetic stimulation modulates neuronal excitability, spine morphology, and Hebbian plasticity in the mouse hippocampus. Hippocampus *0*.

Nicoll, R.A. (2017). A Brief History of Long-Term Potentiation. Neuron *93*, 281–290.

Oliet, S.H.R., Malenka, R.C., and Nicoll, R.A. (1997). Two Distinct Forms of Long-Term Depression Coexist in CA1 Hippocampal Pyramidal Cells. Neuron *18*, 969–982.

Osawa, S., Iwasaki, M., Hosaka, R., Matsuzaka, Y., Tomita, H., Ishizuka, T., Sugano, E., Okumura, E., Yawo, H., Nakasato, N., et al. (2013). Optogenetically Induced Seizure and the Longitudinal Hippocampal Network Dynamics. PLoS ONE *8*, e60928.

Pinel, J.P., and Rovner, L.I. (1978). Electrode placement and kindling-induced experimental epilepsy. Exp. Neurol. *58*, 335–346.

Pinel, J.P., Skelton, R., and Mucha, R.F. (1976). Kindling-related changes in afterdischarge "thresholds." Epilepsia *17*, 197–206.

Racine, R.J. (1972a). Modification of seizure activity by electrical stimulation: II. Motor seizure. Electroencephalogr. Clin. Neurophysiol. *32*, 281–294.

Racine, R.J. (1972b). Modification of seizure activity by electrical stimulation: I. after-discharge threshold. Electroencephalogr. Clin. Neurophysiol. *32*, 269–279.

Racine, R., Okujava, V., and Chipashvili, S. (1972). Modification of seizure activity by electrical stimulation: III. Mechanisms. Electroencephalogr. Clin. Neurophysiol. *32*, 295–299.

Rau, A.R., Chappell, A.M., Butler, T.R., Ariwodola, O.J., and Weiner, J.L. (2015). Increased Basolateral Amygdala Pyramidal Cell Excitability May Contribute to the Anxiogenic Phenotype Induced by Chronic Early-Life Stress. J. Neurosci. *35*, 9730–9740.

Rowley, N.M., and White, H.S. (2010). Comparative anticonvulsant efficacy in the corneal kindled mouse model of partial epilepsy: Correlation with other seizure and epilepsy models. Epilepsy Res. *92*, 163–169.

Santos, S.F., Pierrot, N., and Octave, J.-N. (2010). Network excitability dysfunction in Alzheimer's disease: insights from in vitro and in vivo models. Rev. Neurosci. *21*, 153–171.

Sessolo, M., Marcon, I., Bovetti, S., Losi, G., Cammarota, M., Ratto, G.M., Fellin, T., and Carmignoto, G. (2015). Parvalbumin-Positive Inhibitory Interneurons Oppose Propagation But Favor Generation of Focal Epileptiform Activity. J. Neurosci. Off. J. Soc. Neurosci. *35*, 9544–9557.

Shivacharan, R.S., Chiang, C.-C., Zhang, M., Gonzalez-Reyes, L.E., and Durand, D.M. (2019). Self-propagating, non-synaptic epileptiform activity propagates by endogenous electric fields. Exp. Neurol.

Sloviter, R.S. (1989). Calcium-binding protein (calbindin-D28k) and parvalbumin immunocytochemistry: Localization in the rat hippocampus with specific reference to the selective vulnerability of hippocampal neurons to seizure activity. J. Comp. Neurol. *280*, 183–196.

Spiegel, E.A. (1937). Quantitative determination of the convulsive reactivity by electric stimulation of the brain with the skull intact. J. Lab. Clin. Med. *22*, 1274–1276.

Staba, R.J., Wilson, C.L., Bragin, A., Fried, I., and Engel, J. (2002). Quantitative Analysis of High-Frequency Oscillations (80–500 Hz) Recorded in Human Epileptic Hippocampus and Entorhinal Cortex. J. Neurophysiol. *88*, 1743–1752.

Stover, K.R., Lim, S., Zhou, T.-L., Stafford, P.M., Chow, J., Li, H., Sivanenthiran, N., Mylvaganam, S., Wu, C., Weaver, D.F., et al. (2017). Susceptibility to hippocampal kindling seizures is increased in aging C57 black mice. IBRO Rep. *3*, 33–44.

Swinyard, E.A., Brown, W.C., and Goodman, L.S. (1952). Comparative assays of antiepileptic drugs in mice and rats. J. Pharmacol. Exp. Ther. *106*, 319–330.

Takarae, Y., and Sweeney, J. (2017). Neural Hyperexcitability in Autism Spectrum Disorders. Brain Sci. *7*.

Thiels, E., Barrionuevo, G., and Berger, T.W. (1994). Excitatory stimulation during postsynaptic inhibition induces long-term depression in hippocampus in vivo. J. Neurophysiol. *72*, 3009–3016.

Ting, J.T., and Feng, G. (2013). Development of transgenic animals for optogenetic manipulation of mammalian nervous system function: Progress and prospects for behavioral neuroscience. Behav. Brain Res. *255*, 3–18.

Tischer, D., and Weiner, O.D. (2014). Illuminating cell signalling with optogenetic tools. Nat. Rev. Mol. Cell Biol. *15*, 551–558.

Traub, R.D., and Jefferys, J.G. (1994). Simulations of epileptiform activity in the hippocampal CA3 region in vitro. Hippocampus *4*, 281–285.

Valero, M., Cid, E., Averkin, R.G., Aguilar, J., Sanchez-Aguilera, A., Viney, T.J., Gomez-Dominguez, D., Bellistri, E., and Prida, L.M. de la (2015). Determinants of different deep and superficial CA1 pyramidal cell dynamics during sharp-wave ripples. Nat. Neurosci. *18*, 1281–1290.

Wahlstrom-Helgren, S., and Klyachko, V.A. (2016). Dynamic balance of excitation and inhibition rapidly modulates spike probability and precision in feed-forward hippocampal circuits. J. Neurophysiol. *116*, 2564–2575.

Wang, H., Peca, J., Matsuzaki, M., Matsuzaki, K., Noguchi, J., Qiu, L., Wang, D., Zhang, F., Boyden, E., Deisseroth, K., et al. (2007). High-speed mapping of synaptic connectivity using photostimulation in Channelrhodopsin-2 transgenic mice. ProcNatl AcadSciUSA *104*, 8143–8148.

Wang, Y., Xu, C., Xu, Z., Ji, C., Liang, J., Wang, Y., Chen, B., Wu, X., Gao, F., Wang, S., et al. (2017). Depolarized GABAergic Signaling in Subicular Microcircuits Mediates Generalized Seizure in Temporal Lobe Epilepsy. Neuron *95*, 92-105.e5.

Weitz, A.J., Fang, Z., Lee, H.J., Fisher, R.S., Smith, W.C., Choy, M., Liu, J., Lin, P., Rosenberg, M., and Lee, J.H. (2015). Optogenetic fMRI reveals distinct, frequency-dependent networks recruited by dorsal and intermediate hippocampus stimulations. NeuroImage *107*, 229–241.

Wendling, F., Gerber, U., Cosandier-Rimele, D., Nica, A., De Montigny, J., Raineteau, O., Kalitzin, S., Lopes da Silva, F., and Benquet, P. (2016). Brain (Hyper)Excitability Revealed by Optimal Electrical Stimulation of GABAergic Interneurons. Brain Stimulat. *9*, 919–932.

Williams, J.C., Xu, J., Lu, Z., Klimas, A., Chen, X., Ambrosi, C.M., Cohen, I.S., and Entcheva, E. (2013). Computational Optogenetics: Empirically-Derived Voltage- and Light-Sensitive Channelrhodopsin-2 Model. PLoS Comput Biol *9*, e1003220.

Yeckel, M.F., and Berger, T.W. (1990). Feedforward excitation of the hippocampus by afferents from the entorhinal cortex: redefinition of the role of the trisynaptic pathway. Proc. Natl. Acad. Sci. U. S. A. *87*, 5832–5836.

Yekhlef, L., Breschi, G.L., Lagostena, L., Russo, G., and Taverna, S. (2015). Selective activation of parvalbumin- or somatostatin-expressing interneurons triggers epileptic seizurelike activity in mouse medial entorhinal cortex. J. Neurophysiol. *113*, 1616–1630.

Yizhar, O., Fenno, L.E., Davidson, T.J., Mogri, M., and Deisseroth, K. (2011). Optogenetics in neural systems. Neuron *71*, 9–34.

Yonekawa, W.D., Kupferberg, H.J., and Woodbury, D.M. (1980). Relationship between pentylenetetrazol-induced seizures and brain pentylenetetrazol levels in mice. J. Pharmacol. Exp. Ther. *214*, 589–593.

Zhang, M., Ladas, T.P., Qiu, C., Shivacharan, R.S., Gonzalez-Reyes, L.E., and Durand, D.M. (2014). Propagation of epileptiform activity can be independent of synaptic transmission, gap junctions, or diffusion and is consistent with electrical field transmission. J. Neurosci. Off. J. Soc. Neurosci. *34*, 1409–1419.

Zijlmans, M., Jiruska, P., Zelmann, R., Leijten, F.S.S., Jefferys, J.G.R., and Gotman, J. (2012). High-frequency oscillations as a new biomarker in epilepsy. Ann. Neurol. *71*, 169–178.

Ziskind, E., Sjaardema, H., and Bercel, N.A. (1946). Minimal electroencephalographic response to metrazol as a method for measuring the convulsive threshold for use in human beings. Science *104*, 462.